Chapter -4

4 Protein Nano Dots Conjugated AuNP, Poly-Lysine Bio-interface for the Selective Voltammetric Estimation of Melatonin

4.1 Introduction

Melatonin (Mel) or 5 methoxy-N-acetyltryptamine is an electroactive hormone secreted by the pineal gland that maintains the circadian rhythm of the body by regulating the sleep-wake cycle and keeping track of the clock and calendar in all living organisms, including humans [180]. In a healthy human, the blood Mel level ranges from a few pM to ~ 1400 pM depending on the age group and sampling time [181,182]. The optimum concentration of Mel is responsible for mediating a series of physiological and neuroendocrine processes, and consequently, any imbalance can lead to certain psychiatric, sleep, and mood disorders[183]. Furthermore, an altered level of Mel is also known to influence many other biological behaviors like sexual maturation[184], malignancy[185], bone density[186], cardiovascular functioning, etc.[181]. The substantial role of Mel concentration in maintaining the proper body functioning, therefore, leads to its wide use as a medical supplement[187]. The external administration of 0.1 - 10 mg of Mel as supporting medication for insomnia, jet lag disorders, and anxiety has been profusely suggested by clinicians[188]. Despite not being FDA approved, many studies, including Covid-19 treatment protocols[189,190], have brought the limelight on Mel for its effectiveness in critical care patients by reducing anxiety and improving sleep quality[181].

Nevertheless, the easy availability of Mel as an unprescribed over-the-counter medication in such high doses leads to an increased risk of imbalanced Mel levels that can pose many side effects and cause disturbed body functions[191]. In particular, prolonged melatonin therapy prompts adverse effects in infants[192], prepubescent children, and pregnant and breastfeeding women[193]. Administration of melatonin to patients suffering from renal disorders, impaired liver functioning, or autoimmune diseases are known to pose more chronic adverse effects, which can be sensed through the increased melatonin level in body fluids[194,195]. Therefore, the estimation of melatonin is critically important for both the early diagnosis of many health conditions and for collecting systematic data on the adverse effects of excess dosage under different health conditions. In addition to animal species, melatonin is also present in plants and known as phytomelatonin. Melatonin also plays an essential role as a potential modulator for growth and development in plant cells. Studies show that various physiological and biochemical processes in plants, such as germination, root growth, stem elongation, and fruit and seed development, are mediated by the rapid transport of molecules by melatonin, even in case of drought, heavy metal contamination, extreme weather conditions, fungal and bacterial infection melatonin help plants to survive and grow[196,197].

The low concentration of Mel in biological fluids and the coexistence of other biological compounds make the routine determination analytically challenging[198]. Numerous techniques like immunoassay, fluorimetry, and high-performance liquid chromatography coupled with mass spectrometry have been utilized for ultrasensitive detection of melatonin in human blood serum, urine, saliva, and cerebrospinal fluid[199–201]. Although these techniques offer sensitive and selective assay, but require bulky and costly instrumentation, pre-sample treatment, and skilled personnel to operate, which adds to the cost of the test

and increases the testing time. On the other hand, electrochemical techniques do not require any pretreatment process or preparation and provide excellent sensitivity in a wide range of concentrations, solvents, and temperatures[202]. Furthermore, this method can be utilized for on-the-spot detection of the analytes owing to small-sized instrumentation and ease in device fabrication. In the last decade, several voltammetric techniques like cyclic voltammetry[203], square wave voltammetry[204], and differential pulse voltammetry[205] have been frequently used to detect melatonin using a variety of electrode modifications. ZnO nanorods coated on carbon paste electrode[206], graphene decorated with magnetite and acetylene black-chitosan nanoparticles coated on a gold electrode[207], nanopalladium grained polymer nanocomposite coated on glassy carbon electrode[204] are some of the recent modifications of electrode for melatonin detection using square wave voltammetry. However, previously reported sensors were broadly based on tedious surface modifications or showcased bio-incompatibility, poor selectivity, or sensitivity in a complex matrix[208,209]. Herein, we are proposing the unconventional sensing platform based on protein-derived nanocomposite for the selective electrochemical detection of Mel using voltammetry. Due to the wide availability of precursors in different shapes and sizes, protein-based nanomaterials have attracted massive attention from the research community, especially of those working at biological and material science interfaces[210,211]. Amidst several advantages, like easy fabrication, biocompatibility, high stability, biodegradability, narrow size distribution, etc., the most significant is the presence of several reactive functional groups on their surface[212–214]. These functionalities stem from the variety of amino acids in the precursor protein[215]. It offers numerous possibilities for surface modification via covalent/non-covalent interactions that are beneficial for imparting specific interactions with the analytes of choice. Nevertheless, for the electrochemical applications of these

protein nanodots, the charge transfer kinetics need to be improved. Building on the ease of surface modification of protein-derived nanomaterials, here in this work, we demonstrate a facile electrochemical mean to tailor a poly lysine thin film conjugated with gold nanoparticles and protein nanodots derived from BSA. The single-step surface engineering of BSA-derived nanodots using electrochemical reduction/polymerization of Au-polyLysine nanocomposite was aimed to (1) impart stability by restricting the dissolution of BSA nanodots and (2) overcome the inherently compromised charge transfer. The aforementioned benefits of the proposed surface modification were expected to arise through the covalent interactions between the thiol group of BSA nanodot and AuNPs in the surface modification and the flexible organic backbone of poly-lysine that is significantly stable against dissolution.

Additionally, the active amino groups of the poly-lysine film demonstrate an affinity for the selective interaction with the C-O/C=O groups of the amphiphilic aromatic melatonin molecule leading to its trace detection via facilitated charge transfer when it was applied at bio-interface.Within the frame of our knowledge, the use of protein-derived nanomaterials for the development of voltammetric sensing platforms has not been reported previously. Therefore, to acknowledge the set of proposed facts with the conducted experiments, the following sections present a detailed and systematic study of the design and implication of protein nanodots conjugated AuNP, poly-Lysine bio-interface for the voltammetric estimation of melatonin.

4.2 Results and discussion

4.2.1 Synthesis and Characterization of PNDs

The single-step one-pot hydrothermal method was used to synthesize PNDs using BSA protein at physiological pH. The thermal degradation of the protein solution was achieved by heating at 200°C for 15h leading to a well-dispersed colloidal solution of the protein nanodots. The High-Resolution Transmission Electron Micrograph of the prepared nanodots is presented in Figure 4.1(a). The homogeneous distribution of the nano-sized particles with spherical morphology can be clearly concluded from the TEM image. The particle size distribution histogram of the PNDs is shown in the TEM image's inset, which is centered at 3-4nm. The UV-Vis absorbance spectrum (Figure 4.1 (b)) contains prominent absorbance peaks at 268nm and a broad peak around 325nm. A sharp peak at 268nm corresponds to π -π * electronic transition of C=C and n-π* electronic transition of C=O bond, while a broad peak at 325nm is due to different functional groups on PNDs surface27. Additionally, the blue shift of the peak from ~280nm exhibited by the precursor material to 268nm in the PND colloidal solution indicates the decrease in particle size and formation of nanodots. Zeta potential measurement of the PNDs possesses a negative potential value of -21.2mV, which confers particle stability in an aqueous solution attributed to the repulsion between individual nanodots.

FTIR and XPS measurements were next carried out to study the surface functionality and chemical composition of PNDs. The FTIR spectrum of PNDs is shown in Figure 4.2. The broad band near 3450.45cm^{-1} can be attributed to N-H stretching and/or O-H stretching. The band at 2965.91 & 2873.13cm^{-1} corresponds to C–H vibration. The smaller peak near 2,500cm^{-1} reflected the presence of S–H functionalities on the PND surface. The band centred at 1664.85cm^{-1} and 1540cm^{-1} are characteristic peak of amide I and amide II

indicating the peptide origin of the PNDs. The peak at 1384cm^{-1} can be attributed to C-N stretching mode. The broad band near 702.95 cm^{-1} reflected the wagging mode of -NH_2 & -NH. The band centred at 622.86cm^{-1} can be attributed to lysine in BSA.

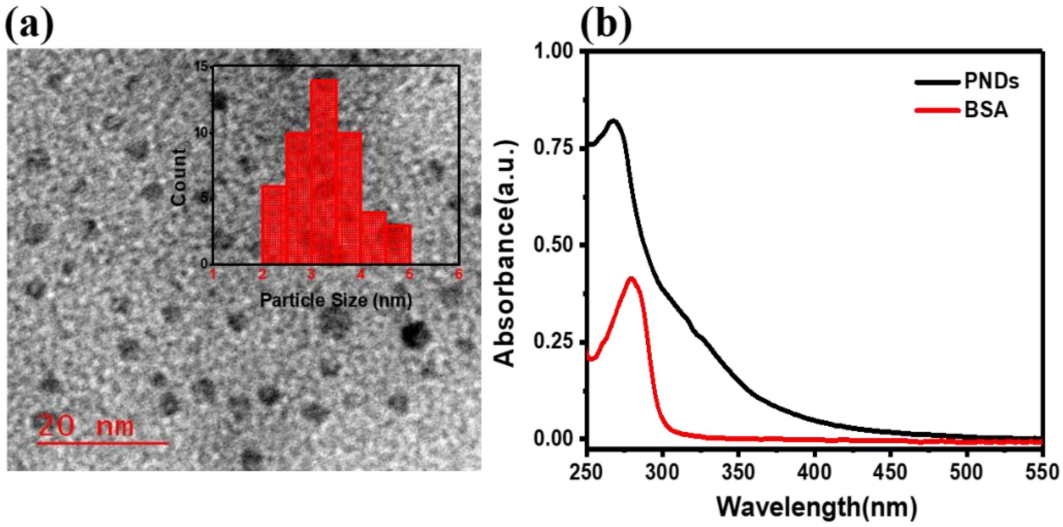

Figure 4.1 (a) TEM image of PNDs at 20nm: histogram shows the average size distribution of PNDs (b) Absorbance spectrum of PNDs and BSA protein in pH-7 buffer

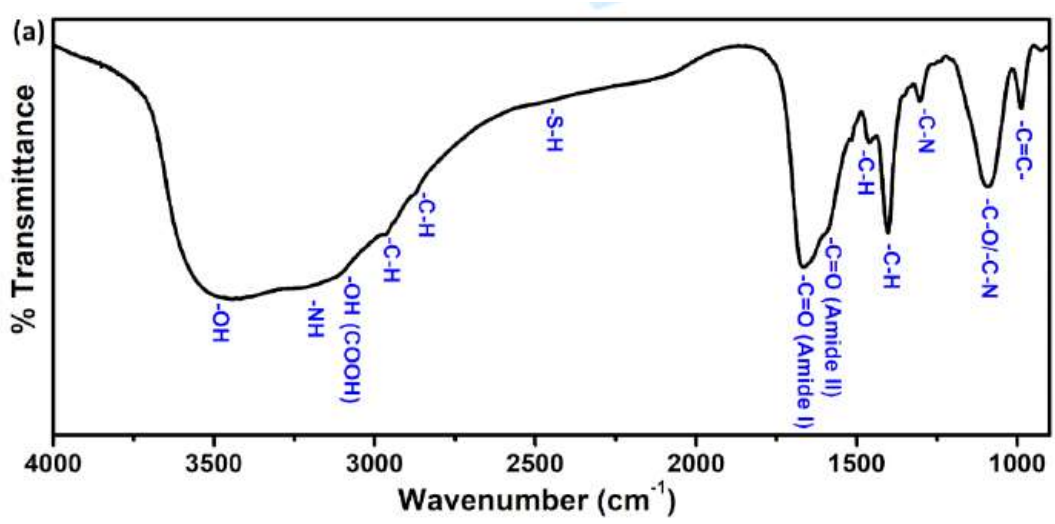

Figure 4.2 Full scan spectrum of FTIR of PNDs

The full scan survey of the XPS spectrum (Figure 4.3 (a)) showed the atomic percentage elemental composition of PNDs. PNDs are mainly composed of carbon, nitrogen, and oxygen with an atomic percentage of 78.34%, 10.53%, and 10.98%, respectively.

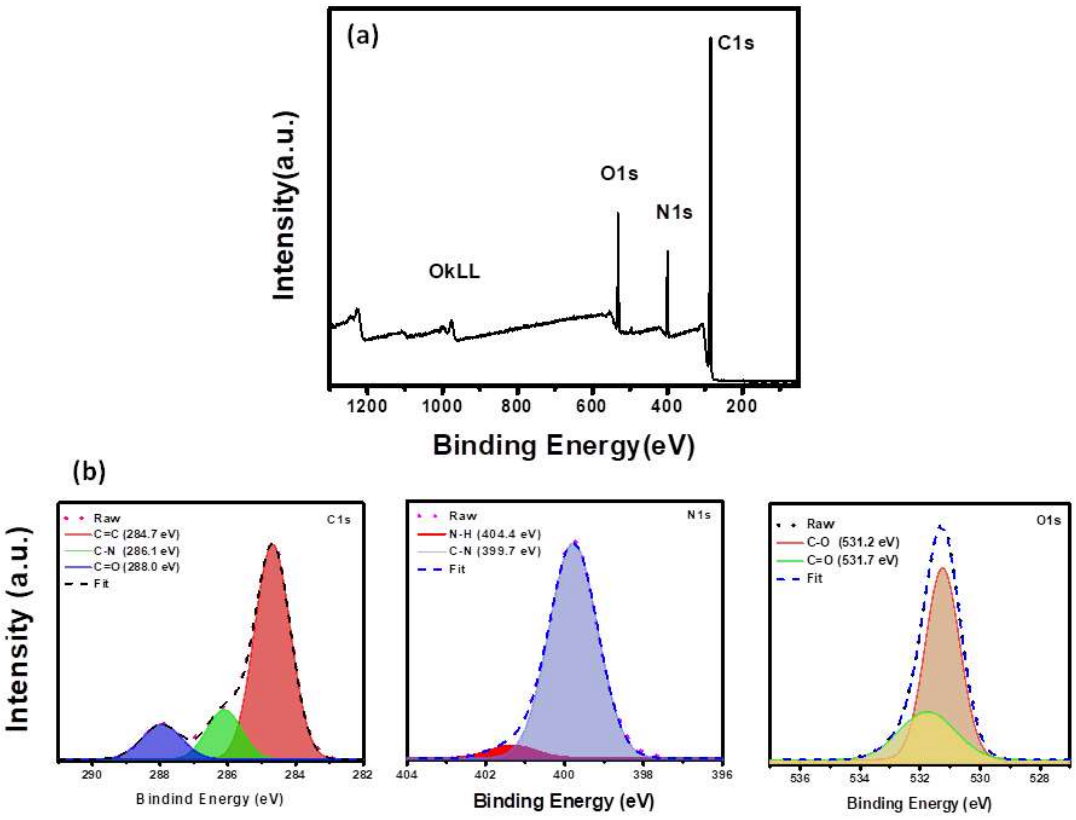

Figure 4.3 (a) Full scan spectrum of XPS spectrum of PNDs (b) Deconvoluted XPS peaks C1s, N1s, O1s

Figure 4.3 (b) shows the deconvoluted peaks of carbon, nitrogen, and oxygen and provides information about the functional moieties present on PNDs surface. The C1s peak was deconvoluted in three peaks at 284.7eV, 288.1eV, and 288.0eV corresponding to C=C, C-N, and C=O bonds, respectively. Similarly, N1s peaks were deconvoluted into two peaks situated at 404.4eV and 399.7eV, which attribute to N-H and C-N bonds, respectively. The O1s peak contains 531.2 and 531.7eV peaks, which mainly corresponds to C-O and C=O

bonds[216]. These functional groups also show their existence in the FTIR spectrum and complement both the analysis techniques. The high degree of an oxygen-containing functional group on the surface leads long term colloidal stability and solubility of PNDs in an aqueous solution. All the characterization acknowledges the formation of protein nanodots of 2-3nm dimensions decorated with many active functional groups stemming from the amino acid backbone of the precursor protein moiety.

4.2.2 PND conjugated AuNP, poly-Lysine Bio-interface: Electrochemical Fabrication and Characterization

To evaluate the electrochemical response of the PNDs, 5µl of PNDs was drop-casted on the polished GCE surface and dried for 1hr at 70°C. The PNDs /GCE was then stabilized by recording continuous voltammograms in pH-7 phospate buffer to remove any unadsorbed PNDs. Figure 4.4 represent the Cyclic voltammogram for 25µM Mel in pH-7 phosphate buffer recorded on bare and modified glassy carbon electrodes. In both cases, the characteristic oxidation peak of Mel appeared at 0.7 V but has different peak current values. In the case of modified electrode higher peak current with a shift towards a lower potential value has been observed which confirm the substantial improvement in sensitivity of the working electrode. Hence, the formation of gold nanoparticle decorated PLL layer on PNDs/GCE surface can effectively accelerate the electrochemical oxidation behaviour of Mel with a significant increase in oxidation current. Attributed to the semiconducting nature of the PNDs, the electrochemical response of Mel on PNDs /GCE was found to be shifted to higher potentials compared to the bare electrode. So, to improve the charge transfer and facilitate melatonin oxidation, the PNDs surface was further engineered by exploiting the available functionalities.

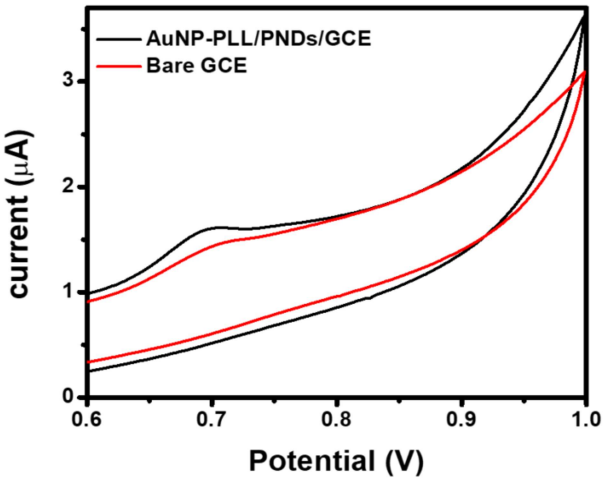

Figure 4.4 Cyclic voltammogram for 25μM Mel in pH-7 phosphate buffer recorded on bare and modified glassy carbon electrodes

Electrodeposition/polymerization of AuNP, Poly-lysine, and AuNP-polylysine nanocomposite directly on the PNDs /GCE was carried out by scanning 15 consecutive cyclic voltammograms (Figure 4.5 (a)) in 1:1 solution of 1mM $HAuCl_4$ and 1 mM L-Lysine within a potential window of -1 to +1.8V at 100mV/s, and the resulting surface is abbreviated as Au-PLL/ PNDs /GCE (For individual AuNP or polylysine coatings, their respective solution were used instead of mixture). As seen from Figure 4.5 (a), the first scan exhibited three main peaks. The peak I at 0.93V corresponds to the growth of gold nanoparticles on the surface during the electrochemical process[217]. Gradual increase in peak current with each scan and potential shifts towards lower values attributed to the oxidation (also termed as activation) of deposited gold nanoparticles from lower oxidation state to higher oxidation state. Whereas peak II at 1.57V was observed only in the first cycle and represents the formation of the radical to initiate polymerization of l-lysine following Hofer-moest reaction or non-Kolbe synthesis in which carboxyl group converts to radical during oxidation[218]. After the first scan, the peak II disappeared indicating the radical

consumption during polymerization leading to the formation of the AuNP-PLL layer on the PNDs/GCE surface. The peak III at -0.37 V corresponds to the reduction of oxygen-containing group localised on the PNDs /GCE surface and was also observed during the stabilization of PNDs/GCE. The increase in the peak current with the increasing scans for the first 7-8 cycles indicates the facilitated redox process due to the surface deposition AuNP-PLL on PNDs particles. To summarize, (a) demonstrates the facile electrochemical tailoring of PNDs with AuNP-PLL nanocomposite in less than 30 minutes without using any extra chemical or reducing/polymerizing agent. To evaluate the most suitable surface modification for Mel sensing, square wave voltammograms were next recorded in 25μM Mel solution. Figure 4.5 (b) shows the comparative electrochemical response of bare GCE, PNDs/GCE, AuNP/PNDs/GCE, PLL/PNDs/GCE, and AuNP-PLL/PNDs/GCE. Substantially improved electrochemical behavior of AuNP-PLL/PNDs/GCE was witnessed compared to all other modifications with a maximum peak current, ~ 2.5 fold higher than bare GCE and a shift of ~ 60mV towards lower potential. The potential shift indicates the eased Mel oxidation at the surface of AuNP-PLL/PNDs/GCE. Other modifications also demonstrated an increase in the peak current or shift in oxidation potential, but they were less significant than AuNP-PLL/PNDs/GCE. Hence, AuNP-PLL/PNDs/GCE was selected as the most appropriate surface modification for the Mel sensing and further investigated in detail.

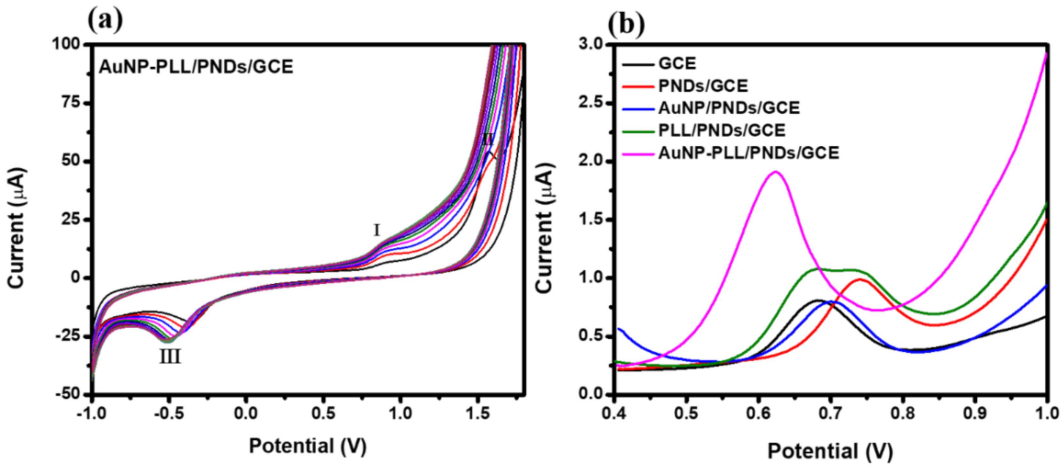

Figure 4.5 (a) Electro-polymerization of PNDs coated GCE in Au:lysine (1:1) solution by 15 scans (b) Square wave voltammograms for different modifications of sensing surfaces

To visualize the changes occurring on the surface during the fabrication process, HR-SEM and HR-TEM images were recorded after repeating the same protocol on ITO pieces. Figure 4.6 (a-c) represents the bare-ITO, PLL-PNDs/ITO, and AuNP-PLL/PNDs/ITO surface, respectively. The images showcase the changes in the surface topography with both the surface modifications. However, it can be clearly seen that in the absence of AuNP, a smooth, thin surface layer of polylysine was observed. On the other hand, in the presence of AuNP, polylysine was assembled in beautiful snowflakes like dendrites demonstrating the visual difference in surface morphologies in the presence and absence of AuNPs. The dendritic like surface is expected to offer more edges and increased active sites, which shall enhance the electrochemical response of the surface deposited electrode. The successful surface modification of the surface was further confirmed through HRTEM (Figure 4.6 d,e). Thin sheets of polylysine conformally decorated with AuNP and protein nanodots were observed. Using EDX and elemental mapping (Figure 4.6, f), the presence of gold was also confirmed. The electroactive surface area of the bare and modified electrode was next evaluated by recording the cyclic voltammograms of bare as well as modified electrode in an equimolar

mixture of 1mM $K_3Fe(CN)_6$ solution & 1M KCl at different scan rates in the range of 10-100mVs^{-1}. The surveyed plots for the bare and modified surface (Figure 4.7 a,b) exhibit an oxidation peak at 0.260V and reduction peak at 0.195V with the peak separation of 0.065V, indicating the quasi-reversible characteristics of the redox couple[219]. No apparent potential shift was observed with the increase in scan rate. The electrochemically active area of bare and modified electrodes was calculated using the Randle Sevcik equation[220],

$$I_p = \pm 2.69 * 10^5 \, n^{\frac{2}{3}} A \, D^{\frac{1}{2}} C \, v^{\frac{1}{2}}$$

Where I_p is the peak current (μA), n is the number of transferred electrons, A is the electro-active area (cm^2), D is the diffusion coefficient of $(Fe(CN)_6)^{3-}$ in KCl solution (cm^2 s^{-1}), C is the concentration of probe molecule (μM) and the υ is the scan rate (V s^{-1}).

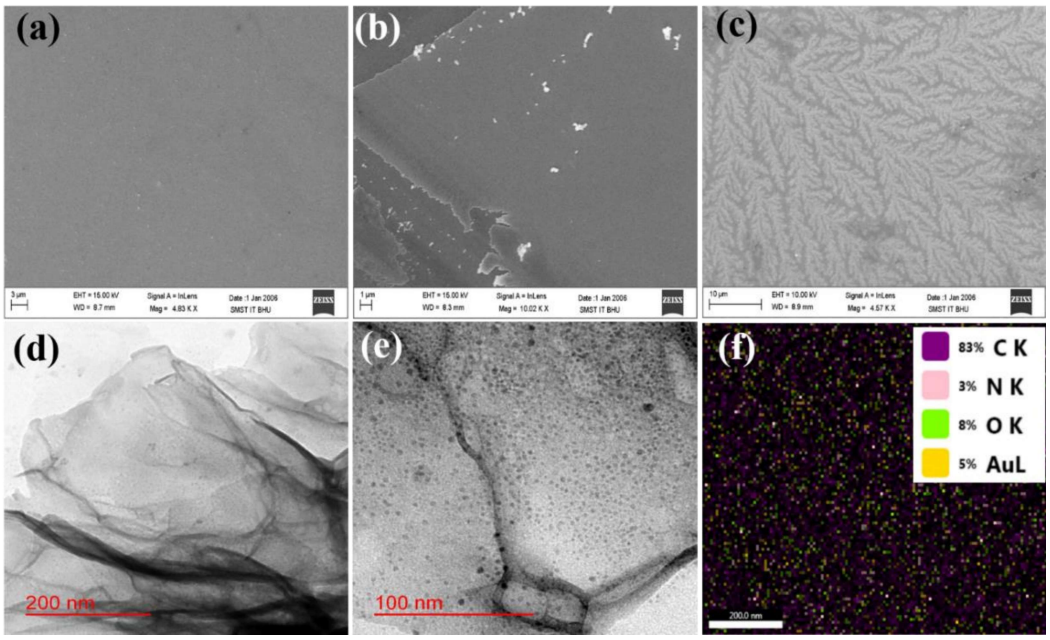

Figure 4.6 SEM images of (a) Bare ITO (b) PLL-PNDs/ITO (c) AuNP-PLL/PNDs/ITO, HRSEM imges of AuNP-PLL/PNDs layer at different resolutions (d) 200nm (e) 100nm (f) Compositional elemental mapping of AuNP-PLL/PNDs layer

The active area of the bare electrode was calculated to be 0.791 cm^2, whereas, for the modified electrode, the area was found to be 0.799 cm^2. In contrast to our expectations, both the electrodes exhibited similar electroactive surface area. However, a substantial increase in the peak currents of Mel was observed when AuNP-PLL/PNDs/GCE was used. This confers that the enhancement in the peak current is not attributed to the changes in the electrochemical surface area during surface engineering but is primarily dictated by the enhanced molecular interactions between the PND conjugated AuNP, poly-Lysine bio-interface and melatonin, which is likely to impart selectivity to the developed sensor. Therefore, the electrochemical performance of the AuNP-PLL/PNDs/GCE towards the Mel oxidation was next evaluated.

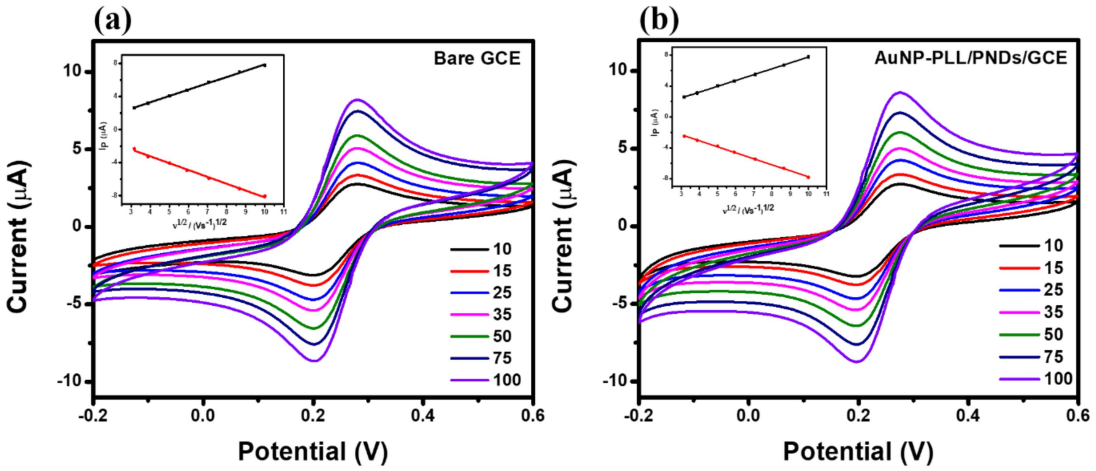

Figure 4.7 Cyclic voltammogram obtained by (a) Bare GCE and (b) AuNP:PLL/PNDs/GCE electrode in presence of 1mM equimolar solution of [Fe(CN6)]3-/4- in 1mM KCL electrolyte solution with varying scan rate from 10-100mV/s-1

4.2.3 Electrochemical Behavior of Melatonin

4.2.3.1 Effect of Concentration

The fabricated AuNP-PLL/PND bio-interface was next investigated to study the electrochemical behavior of melatonin (Mel). To have a calibration plot, the effect of

change in peak current as a function of melatonin concentration was evaluated using square wave voltammetry for both the modified and unmodified electrodes. Sqaure wave voltammograms recorded for different Mel concentrations ranging in between 100nM – 200μM in pH-7 phosphate buffer. A sharp peak at ~ 0.72V in SWV corresponds to the oxidation of melatonin at the bare surface[221]. Whereas, much facilitated Mel oxidation over AuNP-PLL/PND bio-interface was inferred from a shift of ~ 60mV in the peak potential. The shift in the peak potential or the electrocatalytic activity can be assigned to the selective interactions of Mel with the surface modification at the bio-interface leading to aided electron transfer and expedited oxidation at low potentials. Furthermore, with the bare electrode, the lowest concentration that could be visibly detected using SWV plots were found to be 1μM. Interestingly, the AuNP-PLL/PNDs/GCE showed a peak even at 10nM Mel concentration (Figure 4.8)

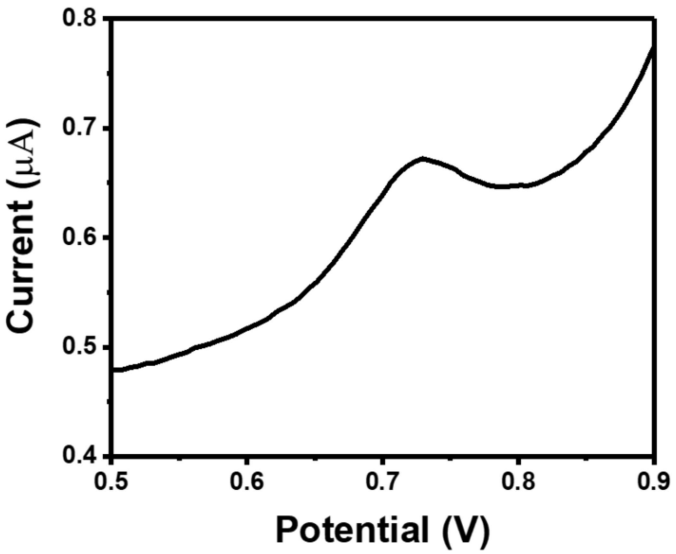

Figure 4.8 Square wave voltammogram of 10nM melatonin concentration

Nevertheless, the concentration dependency could be recognized only above 100nM Mel concentration. The inset of Figure 4.9 shows the linear increase in oxidation peak current Ip with an increase in the Mel concentration for both the bare and AuNP-PLL/PNDs/GCE electrode. However, it was found that the increase in the peak current with increasing concentration is much steeper at lower concentrations (till 25μM) compared to the higher ones. Therefore, the following two linear regression equations were used to express the dependence of Ip on Mel concentration for both the electrodes.

AuNP-PLL/PNDs/GCE: $Y= 0.043\ [0.1\text{-}25\mu M] + 0.2115, \quad R^2 = 0.9948$

$Y= 0.0213\ [50\text{-}200\mu M] + 0.789, \quad R^2 = 0.9998$

Bare GCE: $Y= 0.0194\ [1\text{-}25\mu M] + 0.0171, \quad R^2 = 0.9937$

$Y= 0.009\ [50\text{-}200\mu M] + 0.3818, \quad R^2 = 0.9948$

From the regression equations, it can be concluded that the fabricated bio-interface exhibited an increase of more than two fold in sensitivity compared to the bare electrode. Limit of detection (LOD) for bare and modified GCE was also calculated using 3S/σ, where S stands for a standard deviation of 'n' number of blank voltammograms and σ is the slope of the calibration plot. The LOD for modified GCE was found to be 31.6nM which is reasonably lower than the LOD of bare GCE, which is 120nM.

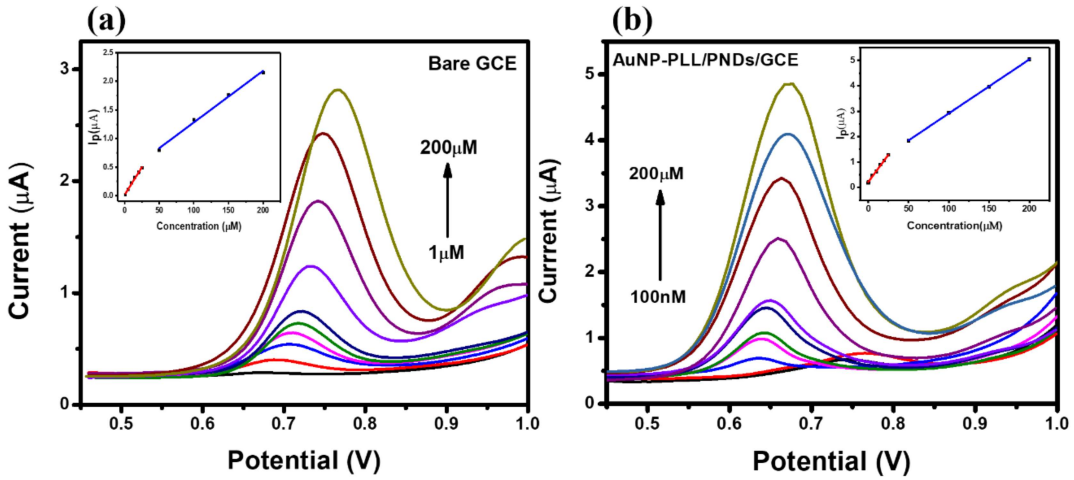

Figure 4.9 Concentration-dependent study: (a) Square wave voltammogram recorded for bare GCE for 1, 5μM, 10μM, 15μM, 20μM, 25μM, 50μM, 100μM, 150μM, 200μM Mel concentration, calibration plots shown in inset for Mel concentration from 1 μM to 200μM. (b) Square wave voltammograms recorded for AuNP-PLL/PNDs/GCE for 100nM, 500nM, 5μM, 10μM, 15μM, 20μM, 25μM, 50μM, 100μM, 150μM, 200μM Mel concentration, calibration plots shown in inset for Mel concentration from 100nM to 200μM

4.2.3.2 Effect of Square Wave Frequency

To study the nature of the mass-transfer process involved in the oxidation of Mel, variation in the oxidation peak current was recorded with increasing frequency (*f*) of the square wave. Figure 4.10 (a) shows the square wave voltammograms corresponding to 25μM Mel in pH-7 buffer with varying frequencies from 5-35Hz. The variation in peak current I_p was plotted as a function of *f* and $(f)^{1/2}$ (Figure 4.10,b) where I_p Vs. $(f)^{1/2}$ showed more linear regression relation in comparison to I_p Vs. *f*.

$$I_p\,(\mu A) = 0.0504\,f\,[5\text{-}35Hz] + 0.6754 \qquad R^2 = 0.9642$$

$$I_p\,(\mu A) = 0.4227\,f^{1/2}\,[5\text{-}35Hz] - 0.1356 \qquad R^2 = 0.9919$$

These results suggest that the oxidation of Mel is diffusion-controlled instead of involvement of any adsorption complications[222].

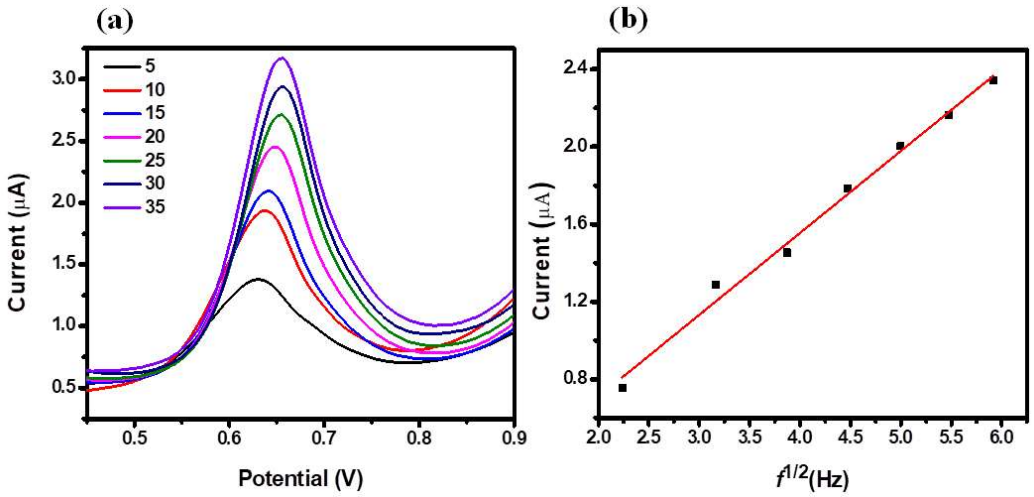

Figure 4.10 (a) Voltammograms for increasing square wave frequency on AuNPs-PLL/PNDs/GCE (b) shows the liner relation between Ip Vs (f) ½

4.2.3.3 Effect of pH

The pH study was next carried out to understand the mechanism of electrochemical oxidation of melatonin. For the study, SWV was recorded in the solution of 25μM melatonin solution prepared using buffer solutions of pH in the range of 2-9. A shift in the peak potential towards lower value was observed with the increasing pH (Figure 4.11,a). This shift of anodic peaks towards a lower potential showcase the facilitation of proton abstraction in basic media[223]. The relation between the peak potential and pH (Figure 4.11,b)can be represented by following linear equation,

$$E_p = - 0.029\ pH + 0.884 \qquad R^2 = 0.99136$$

Being a diffusion controlled process, the oxidation of Mel is assumed to exhibit the nenstian behavior obeying the following equation:

$$E(V) = E^{\circ} - \frac{0.059}{n}\log[\mathrm{H}^{+}]$$

From the Nernst equation expressed above, the slope of E vs pH plot for n = 1 should be 0.059. Therefore, from the slope of the linear equation (dE/dpH) obtained, the number of electrons involved in the electrochemical oxidation of melatonin was found to be ~ 2 (=0.059/0.029) which is in good agreement with the previously reported values.

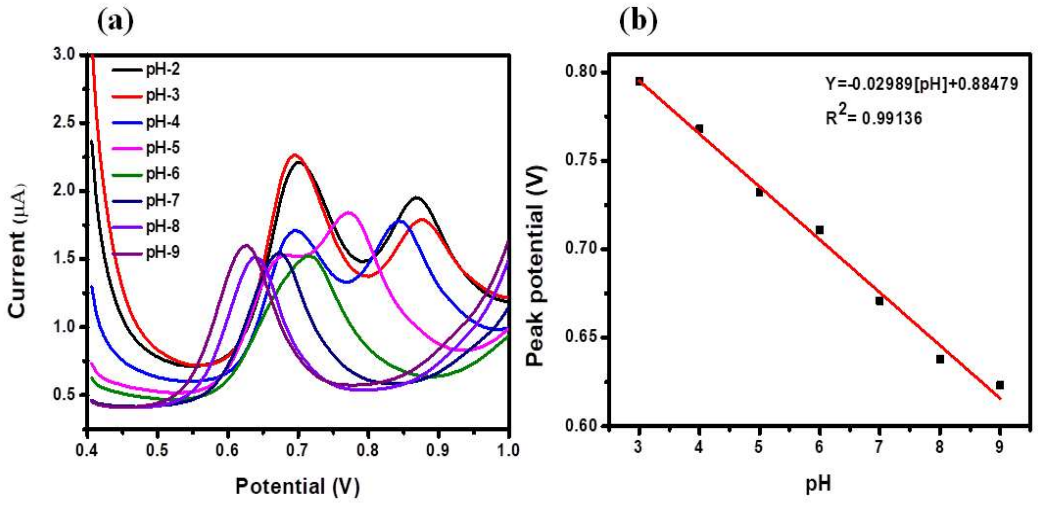

Figure 4.11 (a)Voltammograms for pH of the solution on AuNPs-PLL/PNDs/GCE (b) Effect of pH on AuNPs-PLL/PNDs/GCE

4.2.4 Analytical Application

4.2.4.1 Interference Studies

The estimation of Mel in the complex matrix is majorly challenged by the presence of several other biomolecules like Ascorbic Acid (AA), Uric Acid (UA), and Hypoxanthine (HX) which are commonly present in body fluids as well. Higher concentrations of these metabolites can alter the oxidation peak position and current by interfering in the desired

electrochemical process leading to compromised sensor selectivity. Thus, interference studies have been carried out to investigate the effect of these metabolites.

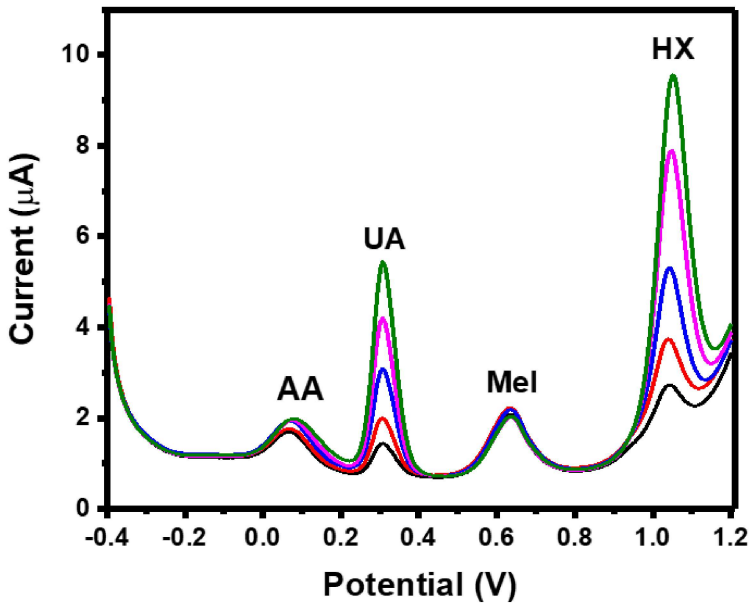

Figure 4.12 Square wave voltammograms were recorded for a fixed concentration of Mel (25μM) with increasing concentration of interference at 12.5μM, 25μM, 50μM, 75μM, 100μM

The SWV voltammograms were recorded for a fixed Mel (25μM) concentration with different concentrations of interference, as shown in Figure 4.12. The AA, UA, and HX oxidation peaks have been observed at 0.06V, 0.30V, and 1.04V, respectively[204]. The recorded voltammograms clearly show that the Mel oxidation peak current and position do not alter even in a high concentration of these interfering metabolites. These results suggest that the modified electrode exhibits promising selectivity and can be used for Mel sensing even in complex matrix and presence of such interfering species.

4.2.4.2 Real Sample Analysis

Pharmaceutical tablet

The modified electrode was utilized to analyze melatonin concentration in the commercially available tablets. For this purpose, a stock solution of 1mM melatonin concentration was made by dissolving the fine powdered tablet in distilled water. The square wave voltammograms were recorded for various tablet concentrations. The table summarizes the observed concentration of melatonin using the calibration chart compared with the sample's actual concentrations. The observed values were found to be in close agreement with the standard concentrations and demonstrated an error of less than 5 %. The concentration, in turn, was also validated using concentration-dependent UV- Vis spectroscopy measurements and exhibited appreciable concurrence with the developed sensor.

Table 4-1 Observed concentration of melatonin using the calibration chart compared with the sample's actual concentrations

Sample	Actual Concentration (µM)	Observed Concentration (µM)	Error (%)
A	25	25.755	3.02
B	50	52.206	4.41
C	100	103.803	3.80

Urine sample preparation

The applicability of the fabricated sensor has been investigated in urine by the standard addition method. Diluted sample (2 ml) of urine was spiked by 500µM stock solution of Mel for desired final concentrations. The square wave voltammograms were recorded with

each spiking of urine shown in Figure 4.13 (a). A weak Mel peak was observed in a diluted urine sample at 0.7V which gets more intense with a gradual increase of Mel concentration. In addition to the Mel peak, the oxidation peak of Uric acid was also observed at 0.4V.

Mung bean Paste

In addition to urine, mung beans paste was also used as a test sample to check the applicability of modified electrode in plants. Crushed mung beans were diluted with pH-7 buffer and directly used for spiking. 2ml of mung bean solution was spiked with a 500µM stock solution of Mel to get the final desired concentration. The square wave voltammograms were recorded with each spiking of Mung bean paste shown in Figure 4.13 (b). Non-spiked mung bean paste showed a small Mel peak at 0.73V with a background peak at 0.86V. The gradual addition of Mel in paste increase the peak current and the calibration plot shows the linear relation between the peak current and Mel concentration. Extrapolation of the obtained cure gives the value of the unknown amount of Mel present in mung bean paste.

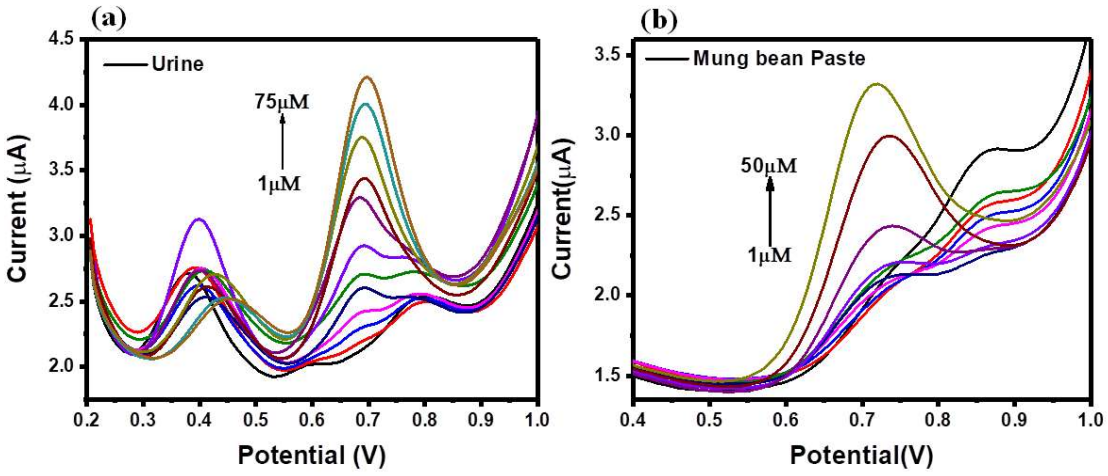

Figure 4.13 (a) Square wave voltammogram of spiked solution of Urine (b) Square wave voltammogram of spiked solution of Mung bean paste

4.2.5 Stability and Reproducibility

The stability of the AuNP-PLL/PNDs/GCE sensing surface was examined by observing the changes in its electrochemical behavior upon excessive cycling in the pH-7 buffer. Figure 4.14 (a) demonstrates the appreciable stability of the fabricated bio-interface over more than 150 cycles. The two peaks observed in Figure 4.14 (a) correspond to the presence of gold nanoparticles and a poly-lysine layer. No substantial change in the shape or the intensity of peaks during the continuous scans confirms the stability of the modified surface for multiple uses. The time-dependent stability and reproducibility of the sensing surface were examined by taking the square wave voltammograms per week in 25µM melatonin solution. The sensing surface showed a < 5 % current drop in the first 15 days and < 9 % after one month when kept open to the air in the lab (Figure 4.14 (b)). The values suggest that the modified surface exhibits excellent stability for a longer duration and does not require extra precautions for storage. However, storing the electrodes in a dry environment or N_2 filled box will increase the lifetime.

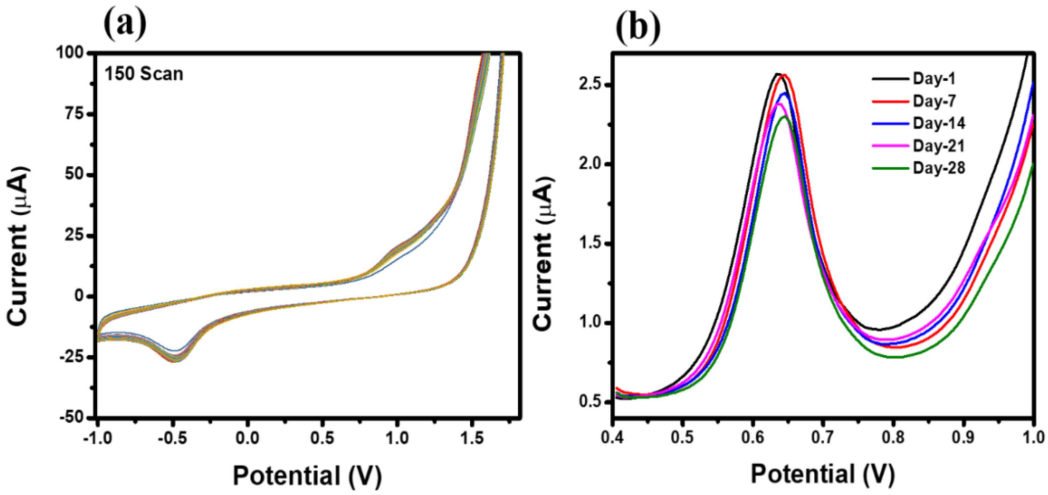

Figure 4.14 (a) Continuous 150 cycle voltammograms of AuNP-PLL/PNDs/GCE (b) Reproducibly of modified sensing surface at different time intervals

4.3 Conclusion

A detailed protocol for the facile fabrication of AuNP-PLL/PNDs/GCE sensor to estimate melatonin has been reported. Utilizing the rich surface functionalities, the BSA derived protein nanodots were electrochemically tailored with AuNP decorated poly-Lysine sheets to overcome their compromised charge-transfer behavior and electrochemical response. The fabricated sensor's chemical and surface characterization has been carried out systematically using HR-SEM, HR-TEM, UV-Vis spectroscopy, FTIR, and XPS. The developed bio-interface was investigated for probing the oxidation mechanism of Mel over electrode surface using CV and SWV. The melatonin was found to oxidize electrochemically, exhibiting a sharp peak at ~ 640mV with a shift of ~ 60mV compared to the oxidation potential of Mel at the bare electrode. The developed sensor demonstrated its efficacy for the quantitative analysis of Mel in a linear range of 0.1 - 200µM with a limit of detection of 31.6nM. The calculated LOD outperformed the previously reported sensors, as summarized in Table 4-2. The as-prepared sensor exhibited excellent selectivity towards melatonin in the test solution, pharmaceutical formulations, and interference matrix. Appreciable stability and reproducibility of the sensor was also evaluated over a period of 28 days. We believe through our work, we open a window for exploring more feasible surface modification strategies to utilize protein-derived nanomaterial for developing stable and selective electrochemical sensors for recognition of biologically relevant molecules.

Table 4-2 Comparison between the performances of reported modified electrodes for melatonin sensing.

Electrode modification	**Standard range**	**LOD**	**Ref.**
Boron doped Diamond electrode	0.5 - 4µM	0.11µM	[208]
ZnO nanorods modified carbon paste electrode	0.3-100µM	750µM	[206]
AHNSA:PdNPs:ErGO/GCE	5 - 100µM	0.09µM	[222]
Palladium nanoparticles decorated carbon aerogel based electrode	0.02 - 500µM	7.1nM	[204]
Cdots/MgNPs/GCE	0.05-13.50µM	0.0044µM	[203]
AB-C modified gold electrode	20-450µM	1.9µM	[205]
AuNPs-PLL /PNDs/GCE	0.1-200µM	31.6nM	This work